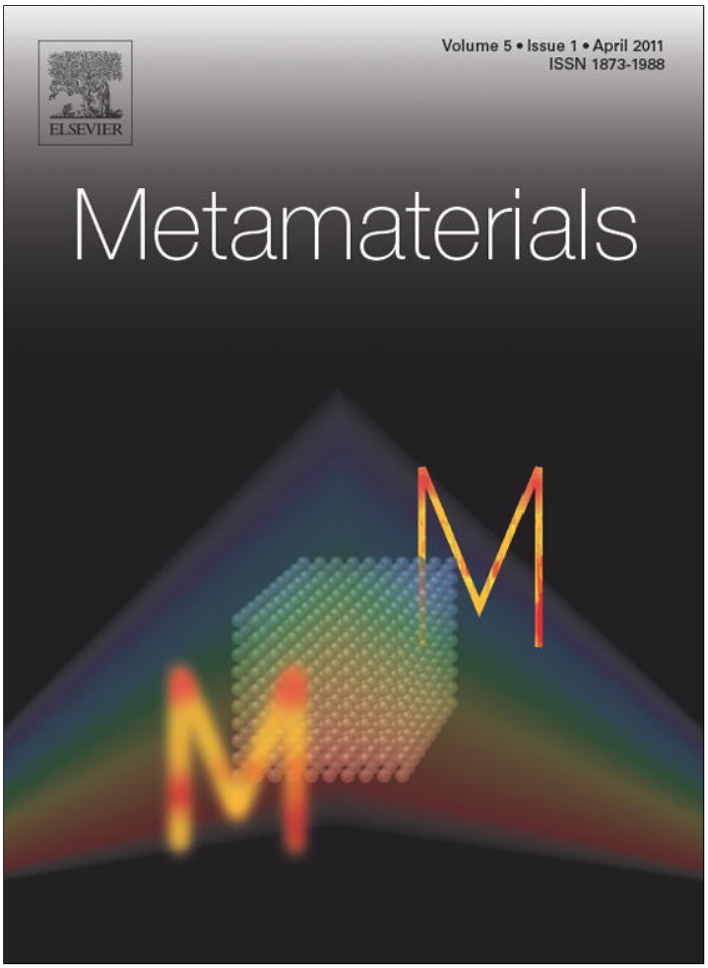

Available online at www.sciencedirect.com
ScienceDirect
Metamaterials 5 (2011) 42–48
Metamaterials
www.elsevier.com/locate/metmat

Coupling transducers for magnetoinductive waveguides: Minimising reflection over the whole pass band

O. Sydoruk

Optical and Semiconductor Devices Group, Department of Electrical and Electronic Engineering, Imperial College London, South Kensington Campus, London SW7 2AZ, UK

Received 2 February 2011; received in revised form 18 February 2011; accepted 20 February 2011
Available online 1 March 2011

Abstract

The characteristic impedance of magnetoinductive waveguides is complex and frequency-dependent, whereas the input impedance of standard RF and microwave devices is real and constant. Transducers capable of coupling magnetoinductive waveguides to other devices are, therefore, required for high-performance magnetoinductive systems. The author designed and experimentally realised a resonant coupling transducer capable of minimising reflections from magnetoinductive waveguides over the whole pass band.

For a magnetoinductive cable with the resonant frequency of 95 MHz and the pass band between 73 and 174 MHz, the experimental value of $|S_{11}|$ was as low as −25 dB at the resonant frequency and about −20 dB over more than 90% of the pass band, the most broadband performance achieved up to date. Yet, the transducer has simple design and comprises only three resonant circuits, which makes it a promising candidate for wide-band applications.

Keywords: Metamaterials; Magnetoinductive waves; Waveguide; Characteristic impedance; Matching; Transducer

1. Introduction

Magnetoinductive waveguides comprise discrete, periodically arranged *LC*-resonators that are magnetically coupled to each other [1]. Introduced in the metamaterial context by Shamonina et al. [2], magnetoinductive devices have been actively studied at RF and microwave frequencies for detection and amplification of MRI signals [3–6], signal processing [7,8], sub-wavelength imaging [9,10,1], soliton propagation [11] and more recently, for data transmission [12] and underground sensor networks [13].

The majority of these applications require connecting magnetoinductive waveguides to other conventional devices. Whereas such devices have real and constant input impedance (usually 50 Ω), the characteristic impedance of magnetoinductive waveguides is complex and frequency-dependent [1]. Coupling transducers are, therefore, needed to match magnetoinductive waveguides to the 50-Ω environment and thus avoid signal reflection. Such transducers were first developed by Syms et al. [14] for waveguides consisting of elements built on printed circuit boards, but the transducers' characteristics were impaired by higher order interactions between the elements [15]. The interaction between next-nearest neighbours could be reduced by using double-sided boards [14], and further progress was possible due to the improved design of magnetoinductive waveguides in the form of thin-film cables [16], where the coupling coefficients between all the elements except the nearest neighbours are substantially reduced. For

E-mail address: o.sydoruk@imperial.ac.uk

1873-1988/$ – see front matter © 2011 Elsevier B.V. All rights reserved.
doi:10.1016/j.metmat.2011.02.003

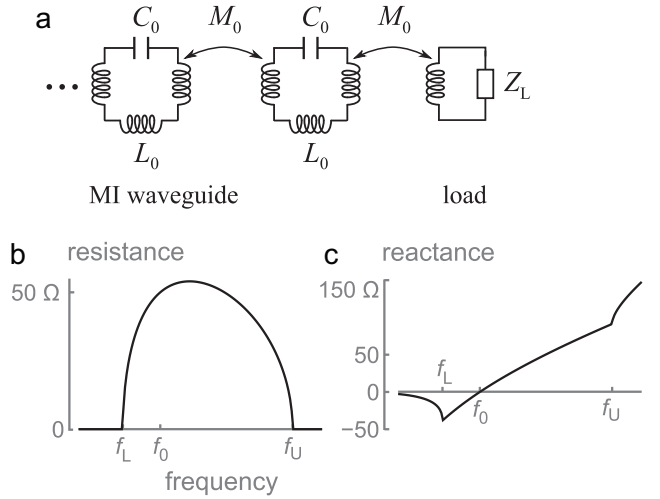

Fig. 1. A reflection-less load magnetically coupled to a magnetoinductive (MI) waveguide (a) has frequency-dependent resistance (b) and reactance (c). The load is purely real at the resonant frequency, f_0, and its resistance is zero at the band edges $f_{U,L}$.

these cables, Syms et al. [17] have developed a resonant transducer that comprised a single *LC*-resonator magnetically coupled to the cable. The transducer provided low reflection of −20 dB over about 60% of the magnetoinductive-wave pass band. Some applications may, however, require transducers with even larger bandwidths.

This paper introduces an improved resonant transducer that can minimise reflection over the whole pass band of a magnetoinductive waveguide. Section 2 presents the design, based on three resonant circuits, and compares it to the single-resonant transducer of Syms et al. [17]. Section 3 reports on experiments with transducers designed for a magnetoinductive cable operating around 100 MHz, and it compares the experimental results with the theoretical predictions. Section 4 draws conclusions.

2. Transducer design

This section discusses a reflection-less matching load for a magnetoinductive waveguide, reviews its realisation based on a single resonant circuit and then presents an improved design based on three resonant circuits.

A magnetoinductive waveguide comprising resonant elements with the self-inductance L_0, the self-capacitance C_0, and the mutual inductance M_0 between the nearest neighbours (see Fig. 1(a)) supports magnetoinductive waves with the dispersion relation [2,1]:

$$1 - \frac{\omega_0^2}{\omega^2} + \kappa \cos ka = 0, \tag{1}$$

where ω is the angular frequency, k is the wave number, a is the period of the waveguide, $\omega_0 = 1/\sqrt{L_0 C_0}$ is the angular resonant frequency of an element and $\kappa = 2M_0/L_0$ is the coupling coefficient. The characteristic impedance of the waveguide is [1]:

$$Z_c = j\omega M_0 e^{-jka}, \tag{2}$$

where j is the imaginary unit. The value of the impedance depends on the frequency and is, generally, complex; it is real only at the resonant frequency, $Z_c = \omega_0 M_0$.

Let a load impedance Z_L be coupled to an end of the waveguide by the mutual inductance M_0, as shown in Fig. 1(a). There will be no reflection from the load if [17]:

$$Z_L = Z_c^*, \tag{3}$$

where the asterix denotes complex conjugation. Substituting Eqs. (1) and (2) into Eq. (3) yields:

$$Z_L = \omega M_0 \sqrt{1 + \frac{Z_0^2}{4\omega^2 M_0^2}} + \frac{Z_0}{2}, \tag{4}$$

where $Z_0 = j\omega L_0 + 1/(j\omega C_0)$ is the self-impedance of an element. In the pass band, the first term of this equation represents the resistance and the second one, the reactance of the load impedance. Both depend on the frequency, as Fig. 1(b) and (c) shows for $R = \omega_0 M_0 = 50\,\Omega$ and $\kappa = 0.7$.

As Syms et al. [17] reasoned, the load reactance of $Z_0/2$ can be realised by an *LC*-resonator with the inductance $L_0/2$ and the capacitance $2C_0$. This resonator will then ideally match the waveguide to 50 Ω at two frequencies, at the resonant frequency, $f_0 = \omega_0/(2\pi)$, and at a frequency above the resonant one (see Fig. 1(b)). Because the load resistance does not change much in the midband, such a resonant transducer will provide broadband matching to a real load. The matching, however, becomes far from ideal near the band edges, f_L and f_U, where the load resistance rapidly decreases (see Fig. 1(b)). (The band edges are determined by $f_{L,U} = \omega_{L,U}/(2\pi) = f_0/\sqrt{1 \pm \kappa}$.)

Better matching at the band edges can be achieved as follows. The 50 Ω impedance, as seen by the waveguide, can be decreased by shunting it with two additional *LC*-circuits, one with the resonant frequency close to f_L and the other one with the resonant frequency close to f_U. The impedance of one of the resonators, and thus the total resistance, will then vanish at the band edges, following the ideal matching resistance shown in Fig. 1(b). Fig. 2(a) shows the equivalent circuit of the corresponding coupling transducer. It consists of three *LC*-circuits, where the first one is responsible for the correct behaviour of the

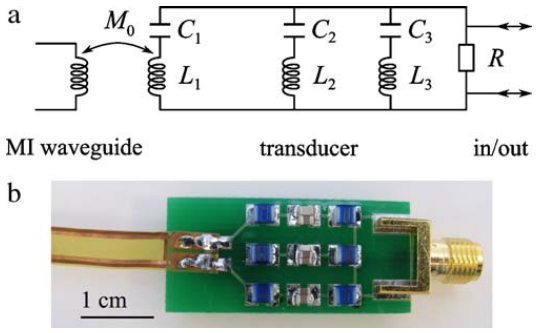

Fig. 2. The resonant transducer comprising three resonant *LC*-circuits [equivalent circuit (a) and photograph (b)] provides good approximation to the ideal load impedance of Fig. 1.

load reactance, and the other two are responsible for the correct behaviour of the load resistance. The values of the inductances $L_{1,2,3}$ and the capacitances $C_{1,2,3}$ should now be chosen in such a way that the total impedance of the transducer matches closely the ideal load impedance, Z_L. Detailed mathematical treatment of the problem is relegated to Appendix A. The final result is

$$L_1 = \frac{L_0}{2} + \frac{R}{2(\omega_y - \omega_x)},$$

$$\frac{1}{C_1} = \frac{1}{2C_0} + \frac{R}{2}\frac{\omega_x\omega_y}{\omega_y - \omega_x},$$

$$L_2 = R\left(\frac{\omega_x}{\omega_x^2 - \omega_{02}^2} - \frac{\omega_y}{\omega_y^2 - \omega_{02}^2}\right), \tag{5}$$

$$C_2 = \frac{1}{L_2\omega_{02}^2},$$

$$L_3 = \frac{1}{\omega_x\omega_y C_2}, \quad C_3 = \frac{1}{\omega_x\omega_y L_2},$$

where

$$\omega_{x,y}^2 = \frac{\omega_0}{2(1-\kappa^2)}\left(2 - \frac{\kappa^2}{4} \pm \sqrt{3\kappa^2 + \frac{\kappa^4}{16}}\right), \tag{6}$$

$$\omega_{02} = 2\omega_L - \omega_x.$$

In agreement with the above expectations, the triple-resonant transducer (Fig. 2) demonstrates low reflection over a wider frequency range compared with the single-resonant transducer of Syms et al. [17]. Fig. 3(a) shows the frequency variation of $|S_{11}|$ for both transducer types; the solid curve is for the triple-resonant transducer and the dashed curve is for the single-resonant one. The variation was calculated as [17]:

$$|S_{11}| = 20\log_{10}|\Gamma|, \tag{7}$$

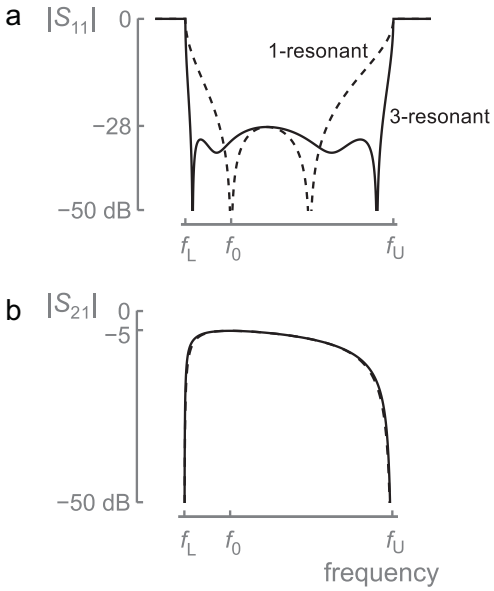

Fig. 3. Compared with the single-resonant transducer (dashed lines), the triple-resonant one (solid lines) provides low reflection over a wider frequency band (a). The transmission characteristics of both transducers are, however, the same over the whole pass band, showing that the transmission is determined by the waveguide loss rather than by reflections.

where $\Gamma = -(Z_L - Z_c)/(Z_L + Z_c^*)$ is the reflection coefficient. The parameters are the same as used for Fig. 1(b) and (c). The maximal value of $|S_{11}|$ of −28 dB is the same for both transducers, but the triple-resonant transducer has a wider frequency band.

However, when $|S_{21}|$ is compared for magnetoinductive waveguides with realistic losses, both transducer types perform similarly. Fig. 3(b) shows the frequency variation of $|S_{21}|$ for the waveguide consisting of 20 elements with the quality factor $Q = 48$ and having the other parameters as in the previous examples. The solid curve for the triple-resonant transducer and the dashed curve for the single-resonant one almost coincide, showing that the amount of power transmitted is dominated by high losses in the waveguide rather than by reflections from the edges. As the quality factor increases, the triple-resonant transducer allows for higher transmission at the band edges, but the improvement is marginal for realistic values of Q up to 200. The values of $|S_{21}|$ were calculated as [17]

$$|S_{21}| = 10\log_{10}\left[(1 - |\Gamma|^2)^2 e^{-2Nk''a}\right], \tag{8}$$

where N is the number of elements, and $k''a \approx 1/(\kappa Q \sin ka)$ is the loss per element.

3. Transducer realisation

This section presents experimental realisation of the triple-resonant transducer for a flexible magnetoinductive waveguide and compares its performance with the theoretical predictions. The waveguide used was a flexible cable whose design and properties are described in detail in Refs. [16,17]. The resonant frequency of the elements was $f_0 = 95$ MHz; their quality factor was $Q = 48$, and the coupling between the nearest neighbours was $\kappa \approx 0.7$. At the resonant frequency, the cable's characteristic impedance was close to 50 Ω. The cable comprised 17 elements and was about 170 cm long. The corresponding transducer parameters calculated from Eq. (5) are $L_1 = 164$ nH, $C_1 = 15.4$ pF, $L_2 = 539$ nH, $C_2 = 9.8$ pF, $L_3 = 205$ nH, $C_3 = 3.7$ pF.

The transducers were made on standard FR-4 printed-circuit boards with copper tracks using surface-mount capacitors and wire-wound inductors. Similarly to the method of Ref. [17], two transducers were connected directly to the inductors that were left on the ends of the cable after cutting it (so that an inductance of approximately $L_0/2 = 120$ nH was connected in series to the first transducer's resonator), see the photograph in Fig. 2(b). The cable with the transducers at both ends was connected to a network analyser (Agilent E5061A) using SMA connectors, and the transducers' characteristics were optimised by varying the capacitors and inductors. Their optimal values were close to the theoretical ones: $L_1' = 32$ nH ($L_1 \approx L_1' + L_0/2$), $C_1 = 13$ pF, $L_2 = 538$ nH, $C_2 = 10.1$ pF, $L_3 = 202$ nH, $C_3 = 3.5$ pF.

The frequency variation of the experimental values of $|S_{11}|$ and $|S_{21}|$ agreed with the theoretical predictions (see Fig. 4). Low values of $|S_{11}| < -19$ dB were achieved experimentally almost for all frequencies between 73 and 166 MHz, which is 93% of the pass band. The reflection is lower (and the agreement between the theory and experiment is better) for the lower part of the pass band, including the resonant frequency, 95 MHz, where $|S_{11}| = -25$ dB. The agreement between the experimental and the theoretical frequency variations of $|S_{21}|$ is, again, better at lower frequencies. The transmission is maximum at the resonant frequency, where $|S_{21}| = -5$ dB both for the theory and the experiment, and the experimental values of $|S_{21}|$ are larger than -10 dB between 75 and 152 MHz.

As one can expect, the transducer could achieve such low experimental values of $|S_{11}|$, because its impedance, as seen by the network analyser, was close to 50 Ω in the whole pass band. Fig. 5 shows the Smith chart of the impedance measured between 50 and 220 MHz. In the pass band, between 72 and 167 MHz, the impedance

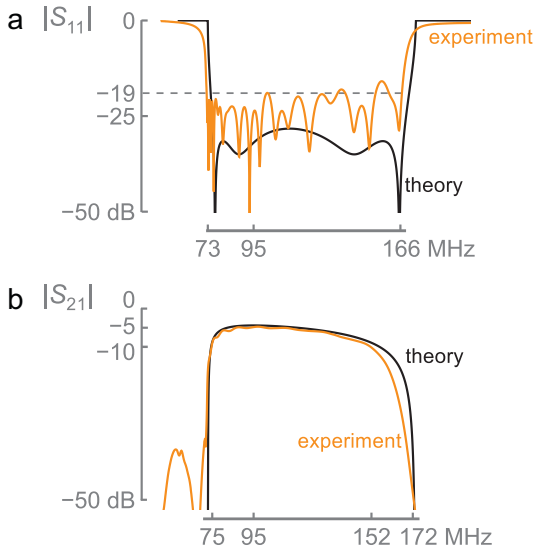

Fig. 4. Low reflection is experimentally observed over 93% of the pass band (a). The theoretical and experimental frequency variations agree both for $|S_{11}|$ (a) and $|S_{21}|$ (b).

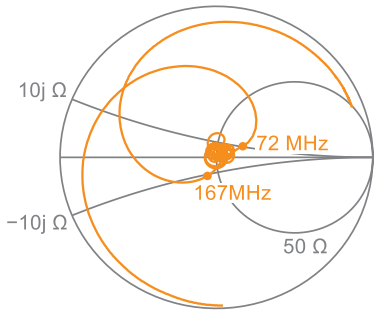

Fig. 5. The measured value of the transducer's impedance, shown on the Smith chart, is close to 50 Ω almost for the entire pass band (between 72 and 167 MHz).

circles around the value of 50 Ω, with both the real and imaginary parts diverging from this point by no more than 10 Ω.

4. Conclusions

Compared with previous designs, the magnetoinductive transducers presented here provide low reflection in a wider frequency range ($|S_{11}|$ is about -20 dB over impressive 90% of the pass band). The improved frequency characteristics are achieved at a cost of a more complicated circuit that comprises three *LC*-resonators. The effort of fabricating the triple-resonant transducers may be worthwhile for applications that require large frequency bands, such as data transmission and parametric amplification [3], or that are sensitive to reflections, for example, high-power transmission. In addition, the design can be used for broadband absorbers, magnetoinductive couplers and power dividers.

When compared with the simple single-resonant transducer of Syms et al. [17], the triple-resonant transducer presents no improvement in the transmission for realistic waveguide loss. The single-resonant transducers should be, therefore, preferred over the triple-resonant one for applications using only the magnetoinductive midband.

Acknowledgements

I thank R.R.A. Syms for proposing the problem, him and T. Floume for help with experiments and for stimulating discussions, and L. Solymar for reading the manuscript and suggesting improvements. I acknowledge financial support by the Royal Society and the Royal Academy of Engineering (Newton International Fellowship).

Appendix A. Determining the values of the elements constituting the transducer

This appendix presents a derivation for the values of the inductances $L_{1,2,3}$ and capacitances $C_{1,2,3}$ that constitute the triple-resonant transducer. The transducer's impedance can be written as (see Fig. 2(a)):

$$Z_T = Z_1 + \frac{R}{1 + R((Z_2 + Z_3)/(Z_2 Z_3))}, \tag{A.1}$$

where $Z_i = j\omega L_i + 1/(j\omega C_i)$, $i = 1, 2, 3$. The values of the inductances and capacitances should be chosen so that the transducer's impedance Z_T is close to the ideal load impedance Z_L (see Fig. 1(b) and (c)). An accurate mathematical formulation of the problem would be too complicated to treat analytically (see, however, the end of this section for numerical calculations). Therefore, I will solve the problem using several heuristic arguments about the properties of the transducer's impedance (Eq. (A.1)). These arguments will lead to simple analytical expressions that yield the values of the parameters close to those derived from exact numerical calculations.

The first argument is: for good matching, the reactance of Z_T should match that of Z_L. The reactance of Z_L in the pass band is $Z_0/2$ (see Eq. (4)) and therefore, one has:

$$\frac{Z_0}{2} = Z_1 + \mathrm{Im}\frac{R}{1 + R((Z_2 + Z_3)/(Z_2 Z_3))}. \tag{A.2}$$

Because Z_2 and Z_3 are zero at the band edges, they have opposite signs in the pass band, and the sum $Z_1 + Z_2$ will be zero at the frequency in the midband defined as

$$\omega_{23}^2 = \frac{C_2 + C_3}{(L_2 + L_3)C_2 C_3}. \tag{A.3}$$

Near this frequency $Z_1 + Z_2 \approx j0$, and the second term on the right-hand side of Eq. (A.1) can be expanded as

$$\frac{R}{1 + R((Z_2 + Z_3)/(Z_2 Z_3))} \approx R - R^2 \frac{Z_2 + Z_3}{Z_2 Z_3}. \tag{A.4}$$

Substituting this equation into Eq. (A.2) yields:

$$\frac{Z_0}{2} = Z_1 - R^2 \frac{Z_2 + Z_3}{Z_2 Z_3}. \tag{A.5}$$

It follows that the second term in this equation should behave like an LC-circuit, which requires $Z_2 Z_3 \approx \mathrm{const}$ over the widest frequency range possible. Because this range should include ω_{23} (Eq. (A.3)) one can write:

$$Z_2(\omega_{23} + \Delta) Z_3(\omega_{23} + \Delta) = \mathrm{const}, \tag{A.6}$$

where $|\Delta| \ll \omega_{23}$. Expanding the terms in Eq. (A.6) into series, neglecting the terms proportional to Δ^2, and denoting $W_i = L_i + 1/(\omega_{23}^2 C_i)$, one can write:

$$\begin{aligned} &Z_2(\omega_{23}+\Delta) Z_3(\omega_{23}+\Delta) \approx \\ &Z_2(\omega_{23}) Z_3(\omega_{23}) + j\Delta[Z_2(\omega_{23}) W_3 + Z_3(\omega_{23}) W_2]. \end{aligned} \tag{A.7}$$

According to Eq. (A.6), this expression must be constant, which is possible if $Z_2 W_3 + Z_3 W_2 = 0$ yielding

$$C_2 L_3 = C_3 L_2, \tag{A.8}$$

and recalling Eq. (A.3), one can write

$$\omega_{23}^2 = \frac{1}{L_2 C_3} = \frac{1}{L_3 C_2}. \tag{A.9}$$

Considering now the real part of Eq. (A.4), one gets, quite expectedly:

$$R = \omega_0 M_0. \tag{A.10}$$

The second argument is: $Z_T = Z_L$ at two frequencies, where $\mathrm{Re} Z_L = R/2$. This argument follows from the requirement of broadband matching. As seen from Fig. 2(b), the frequencies where the load resistance decreases by half are close to the band edges. At these frequencies, reflection from the transducer will be absent, and as a result, reflection near the band edges will be low. The frequencies are determined from the condition:

$$\frac{1}{Z_2} + \frac{1}{Z_3} = \pm\frac{1}{jR}. \tag{A.11}$$

Then, matching the real parts of Z_T and Z_L yields

$$\omega M_0 \sqrt{1 + \frac{Z_0^2}{4\omega^2 M_0^2}} = \frac{R}{2}. \tag{A.12}$$

Solution of this equation gives the expressions for two frequencies, $\omega_{x,y}$ (see Eq. (6)). On the other hand, matching the imaginary parts Z_T and Z_L yields:

$$\begin{aligned} \frac{j\omega_x L_0}{2} + \frac{1}{j\omega_x 2C_0} &= j\omega_x L_1 + \frac{1}{j\omega_x C_1} + j\frac{R}{2} \\ \frac{j\omega_y L_0}{2} + \frac{1}{j\omega_y 2C_0} &= j\omega_y L_1 + \frac{1}{j\omega_y C_1} - j\frac{R}{2} \end{aligned} \tag{A.13}$$

from which C_1 and L_1 can be determined as

$$\frac{1}{C_1} = \frac{1}{2C_0} + \frac{R}{2}\frac{\omega_x\omega_y}{\omega_y - \omega_x}. \tag{A.14}$$

and

$$L_1 = \frac{L_0}{2} + \frac{R}{2(\omega_y - \omega_x)}. \tag{A.15}$$

The third argument is: the reactance of the transducer equals that of the ideal load at the frequency ω_{23}, $Z_T(\omega_{23}) = Z_L(\omega_{23})$. It yields, taking Eqs. (A.14) and (A.15) into account:

$$\frac{Z_0}{2} - Z_1 = -\frac{R}{2(\omega_y - \omega_x)}\left(j\omega + \frac{\omega_x\omega_y}{j\omega}\right). \tag{A.16}$$

This expression becomes zero when $\omega^2 = \omega_x\omega_y$, at the frequency where $Z_1 + Z_2 = 0$. This frequency is determined by Eq. (A.3) as

$$\omega_{23}^2 = \omega_x\omega_y. \tag{A.17}$$

and, from Eq. (A.13):

$$\frac{1}{L_2C_3} = \frac{1}{L_3C_2} = \omega_x\omega_y. \tag{A.18}$$

Then, Eq. (A.11) takes the form:

$$\frac{1}{Z_2(\omega_x)} - \frac{1}{Z_2(\omega_y)} = \frac{1}{jR} \tag{A.19}$$

yielding:

$$L_2 = R\left(\frac{\omega_x}{\omega_x^2 - \omega_{02}^2} - \frac{\omega_y}{\omega_y^2 - \omega_{02}^2}\right). \tag{A.20}$$

The final argument relates the resonant frequencies $\omega_{02,03}$ with $\omega_{x,y}$ and $\omega_{U,L}$: $\omega_x - \omega_L = \omega_L - \omega_{02}$ and $\omega_y - \omega_U = \omega_U - \omega_{03}$. Obviously, ω_x is close to ω_L and ω_y is close to ω_U. From Eq. (6), $\omega_x \approx \omega_L + \delta$ and $\omega_y \approx \omega_U - \delta$, leading to

$$\frac{L_3}{L_2} = -\frac{\omega_y(\omega_x^2 - \omega_{02}^2)}{\omega_x(\omega_y^2 - \omega_{03}^2)}, \tag{A.21}$$

On the other hand, using Eq. (A.9):

$$\frac{\omega_{02}^2}{\omega_{03}^2} = \frac{L_3C_3}{L_2C_2} = \frac{L_3C_3L_3}{L_2L_2C_3} = \frac{L_3^2}{L_2^2}. \tag{A.22}$$

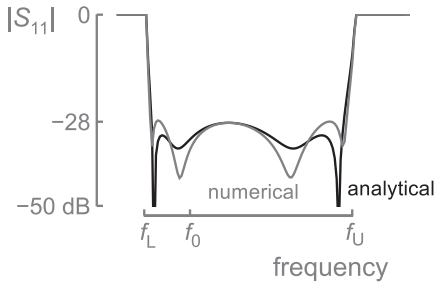

Fig. A.1. Analytical calculations (black) and numerical optimisation (grey) yield similar frequency variations of $|S_{11}|$.

Eqs. (A.21) and (A.22) give the same result if $\omega_{02} = \omega_L - \delta$ and $\omega_{03} = \omega_U + \delta$, which leads to

$$\omega_{02} = 2\omega_L - \omega_x = \frac{\omega_L^2}{\omega_x}, \tag{A.23}$$

Eqs. (A.9), (A.10), (A.14), (A.15), (A.18), (A.20), and (A.23) give the values for the inductors and capacitors of the transducers, summarised in Eq. (5). Although this analytical approach is heuristic, the parameters obtained from Eq. (5) are very close to those derived from numerical calculations minimising the reflection coefficient over the magnetoinductive pass band. Fig. A.1 shows the comparison between the frequency variations of $|S_{11}|$ calculated analytically and numerically (the parameters are the same as in Fig. 2). The numerical calculations minimised the expression $\sum_i |Z_0(\omega_i)^* - Z_T(\omega_i)|^2$ in 2000 frequency points between ω_L and ω_U using the Matlab function "`lsqnonlin`". Remarkably, the two curves have the same broadband behaviour and close maxima and minima of $|S_{11}|$.

References

[1] L. Solymar, E. Shamonina, Waves in Metamaterials, Oxford University Press, 2009.

[2] E. Shamonina, V.A. Kalinin, K.H. Ringhofer, L. Solymar, Magnetoinductive waves in one, two, and three dimensions, J. Appl. Phys. 92 (2002) 6252–6261.

[3] O. Sydoruk, V. Kalinin, E. Shamonina, Parametric amplification of magnetoinductive waves supported by metamaterial arrays, Phys. Stat. Sol. (B) 244 (2007) 1176–1180.

[4] O. Sydoruk, E. Shamonina, L. Solymar, Parametric amplification in coupled magnetoinductive waveguides, J. Phys. D: Appl. Phys. 40 (2007) 6879–6887.

[5] R.R.A. Syms, L. Solymar, I.R. Young, Three-frequency parametric amplification in magneto-inductive ring resonators, Metamaterials 2 (2008) 122–134.

[6] R.R.A. Syms, T. Floume, I.R. Young, L. Solymar, M. Rea, Flexible magnetoinductive ring mri detector: design for invariant nearest-neighbour coupling, Metamaterials 4 (2010) 1–14.

[7] M.J. Freire, R. Marques, F. Medina, M.A.G. Laso, F. Martin, Planar magnetoinductive wave transducers: theory and applications, Appl. Phys. Lett. 85 (2004) 4439–4441.

[8] I.S. Nefedov, S.A. Tretyakov, On potential applications of metamaterials for the design of broadband phase shifters, Microw. Opt. Technol. Lett. 45 (2005) 98–102.
[9] M.J. Freire, R. Marques, Planar magnetoinductive lens for three-dimensional subwavelength imaging, Appl. Phys. Lett. 86 (2005) 182505.
[10] R. Marques, F. Martin, M. Sorolla, Metamaterials with Negative Parameters: Theory, Design, and Microwave Applications, Wiley–Interscience, Hoboken, NJ, 2008.
[11] I.V. Shadrivov, A.A. Zharov, N.A. Zharova, Y.S. Kivshar, Nonlinear magnetoinductive waves and domain walls in composite metamaterials, Photonics Nanostruct.: Fundam. Appl. 4 (2006) 69–74.
[12] C.J. Stevens, C.W.T. Chan, K. Stamatis, D.J. Edwards, Magnetic metamaterials as 1-D data transfer channels: an application for magneto-inductive waves, IEEE Trans. Microw. Theory Tech. 58 (2010) 1248–1256.
[13] Z. Sun, I.F. Akyildiz, Magnetic induction communications for wireless underground sensor networks, IEEE Trans. Antenn. Propag. 58 (2010) 2426–2435.
[14] R.R.A. Syms, I.R. Young, L. Solymar, Low-loss magneto-inductive waveguides, J. Phys. D: Appl. Phys. 30 (2006) 3945–3951.
[15] R.R.A. Syms, O. Sydoruk, E. Shamonina, L. Solymar, Higher order interactions in magneto-inductive waveguides, Metamaterials 1 (2007) 44–51.
[16] R.R.A. Syms, L. Solymar, I.R. Young, T. Floume, Thin-film magnetoinductive cables, J. Phys. D: Appl. Phys. 43 (2010) 055102.
[17] R.R.A. Syms, L. Solymar, I.R. Young, Broadband coupling transducers for magneto-inductive cables, J. Phys. D: Appl. Phys. 43 (2010) 285003.